THE PUBLISHING HOUSE
OF THE ROMANIAN ACADEMY

PROCEEDINGS OF THE ROMANIAN ACADEMY, Series A,
Volume 21, Number 4/2020, pp. 337–355

ROBOTICS ELECTRIC ACTUATORS: RECENT PROGRESS IN HIGH TORQUE DENSITY DESIGNS AND THEIR ADVANCED MOTION CONTROL – A REVIEW

I. BOLDEA[1,2], L.N. TUTELEA[1,2], N. MUNTEAN[1,2], A. POPA[1], F. BLAABJERG[3]

[1] "Politehnica" University Timisoara, Department of Electrical Engineering
[2] Romanian Academy – Timisoara Branch
[3] Aalborg University, Department of Energy Technology, Denmark

Corresponding author: Ana POPA, E-mail: anamoldovan2003@yahoo.com

Abstract. This tutorial review paper intends to introduce performance indexes for robotics electric brushless actuator drives and then synthesize recent progress in their higher torque density designs and advanced motion (position, speed torque) robust control, with representative case study results.

Higher torque density designs refer to a few competitive PMSM topologies, the active materials, characterization and FEMM embedded optimal design methodologies for variable speed operation: low torque ripple is dedicated special attention with sample competitive results. Then, in respect to advanced motion control, field oriented control (FOC), direct torque and flux control (DTFC), feedback linearized control (FLC) and model predictive robust control (MPRC) with encoderless operation are all treated in detail. For control robustness "super-twisting sliding mode" (ST-SM) usage regulators is treated with case studies. For fault tolerance the 2x3 phase twin inverter system is emphasized. Specifying that the micro-robotics electric actuators – as microelectric – mechanical systems – have not been treated here as they constitute today a distinct field with strong peculiarities, we hope that the tutorial review here will be of assistance especially to the new comer to the field of humanoid and industrial robotics electric actuator drives.

Key words: robotics, brushless actuator, super-twisting sliding mode, robust control, optimal design, encoderless operation.

1. INTRODUCTION

Recent progress in digital electric automation and industrial informatics has already led to a strong penetration of robots in many industries: from microrobots through humanoid robots and industrial robots (Fig. 1). However, the very aggressive markets for robots are yet to come soon as a paradigm shifting technology.

a) 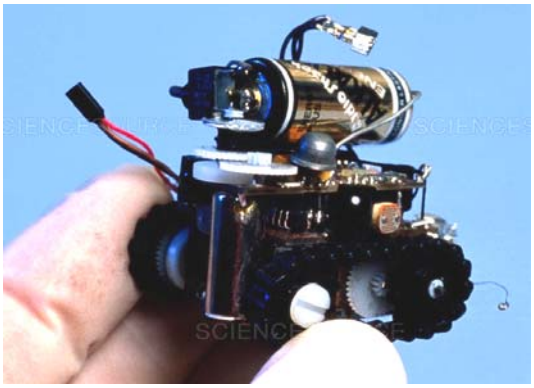 b)  c) 

Fig. 1 – Typical robots: a) micro (https://www.sciencesource.com/archive/Microrobot-SS2313873.html), b) humanoid (https://spectrum.ieee.org/automaton/robotics/humanoids/humanoid-robots-rise), c) industrial (https://new.abb.com/products/robotics/industrial-robots/irb-1410).

All robots are characterized by planned motion position, speed, torque – control in 1, 2, 3 dimensions with an electric actuator dedicated to each direction of motion or even with unique rotary plus linear or spherical electric actuators for multiple dimensional motion integration.

Most robotics literature concentrated so far, rightfully so, on the mission profile, motion trajectory planning and tracking. In general a robot includes a few electric (or hydraulic or pneumatic) actuators coherently controlled for a target trajectory.

So far the d.c. brush PM actuator was routinely used due to its simpler control with fast torque (current) response, starting from any rotor position, in spite of its mechanical commutator problems (scintillation – prone, electromagnetic interference – prone, the wearing of brushes, etc.).

To alleviate these problems but also to provide for higher torque density (in Nm/liter or kg) at good/better efficiency, the brushless a.c. actuators have been vigorously investigated lately and are already in incipient commercial stages. The rapid recent development in power electronics lead to PWM four quadrant (or bidirectional) static power converters with MOSFETs or IGBTs (recently with SIC) of higher and higher power density (higher kVA/liter) and higher efficiency (above 0.97), suitable for multi (3 or 2x3 in general) phase a.c. PM actuator very competitive drives for robotics.

The present review paper aims a synthesis on recent progress in electric PM actuators for robotics: from tentative performance indexes (section II), through high torque density electric PM actuator designs (section III), and their advanced motion control strategies (section IV).

2. PERFORMANCE INDEXES

Borrowing from electric drives heritage [1], a set of performance indexes for robotics electric PM actuators may be introduced to provide solid metrics for fair practical comparisons of different configurations. Here such a tentative set is provided, divided in 3 categories.

2.1. Energy conversion indexes

– Actuator copper loss/Nm;
– Power brushless a.c. electric actuator efficiency η and power factor $\cos\varphi_1$;
– Energy efficiency for dynamic mission profiles (energy output/energy input);
– Electric actuator + PWM converter power (and energy) efficiency;
– Ratio which defines the PWM converter kVA (its cost, etc) – kW/kVA.

2.2. Response indexes

– Plus/minus full torque response time t_s at standstill (in general in the millisecond range);
– Torque ripple ratio $\Delta T/T_{\max}$ – less than 1% in special applications, but less than (5–7)% in general
– Peak torque (inertia ideal acceleration time t_a to base speed on no load);
– Field weakening (constant power) range –CPSR–: $\omega_{\max}/\omega_b$;
– Variable speed range $\omega_{\max}/\omega_{\min}$: in general $\omega_{\max}/\omega_{\min} > 200/1$ in robotics, which qualifies their electric actuators mostly in the servodrive category;
– Thermal limitation; depends on application but in precision position tracking tasks: $\theta_{\text{actuator}} < (20–30)^\circ\text{C} + \theta_{\text{ambient}}$;
– Noise/vibration level in dB: $L_{\text{noise}} \approx 70 + 20\log(P_{\text{re}}/P_{\text{n0}})$; $P_{\text{n0}} = 1$ kW;
– Motion control steady state precision: ΔT_e (in p.u.), $\Delta\omega_r$ (in rpm), rotor position $\Delta\theta_r$ (in degrees);
– Motion control robustness against electric actuator parameter variation: $\Delta T_e/\Delta P_{ar}$, $\Delta\omega_r/\Delta P_{ar}$, $\Delta\theta_r/\Delta P_{ar}$ or against the total rotor inertia (of electric actuator plus load) and against load variations;
– Dynamic stiffness Δs: error against given torque perturbation: $\Delta s = \Delta T_{\text{perturbation}}(\omega)/\Delta x$, with x the variable error, versus perturbation frequency ω.

2.3. Specific weights and costs

– Electric actuator torque densities: Nm/kg, Nm/liter of active materials;
– Active materials cost per Nm of torque;
– PWM converter kVA/liter, kVA/kg;
– Ownership cost USD/kVA;
– Costs of electric actuator system:

$C_{total} = C_{equipment} + C_{loss} + C_{maintenance}$ over dominant duty cycles along entire actuator system life.

As expected, various applications require part of the above indexes in the electric actuator system specifications while new applications may need also new ones. Again, the above tentative performance indexes are not be considered unique but only orientative; however many of them will "surface" in the following sections as the recent progress is closely related to them. We will start now treating "the high torque density designs".

3. ROBOTICS ELECTRIC ACTUATORS HIGH TORQUE DENSITY DESIGNS

Due to space limitations we will skip entirely recent progress in d.c. brush PM electric actuators design and control and small-medium cage-rotor induction (a.c., brushless) electric actuators because higher torque density is obtained with PM brushless electric actuators with a single rotor or with a double rotor (magnetic geared). Also, we will restrict ourselves to robotics electric actuator systems with maximum speeds of 1000-2000 rpms and torques in the range of about 0.1–100 Nm as they seem most common for humanoid and industrial robots. This way electric actuator designs with tens of poles may be considered for a fundamental frequency of less than 500 Hz that limits both core losses in the actuator and the commutation losses in the PWM converter.

All PM brushless actuators considered here are a.c. multi (or single) phase small electric motors. Most of them make use of flux – modulation (variable reluctance) in order to offer magnetic gear (torque magnification) effects both in single or dual rotor topologies [2]. Finally, the purely reluctance and the d.c. excited synchronous motors are also left out due to their lower torque density.

Thus only a few strong competitors are presented below:

3.1. Outer or inner rotor non-overlapping winding PM brushless actuators?

Outer surface – PM – rotor interior – stator PM brushless actuators (Fig. 2) have been analyzed recently as strong candidates for higher torque density [3, 5].

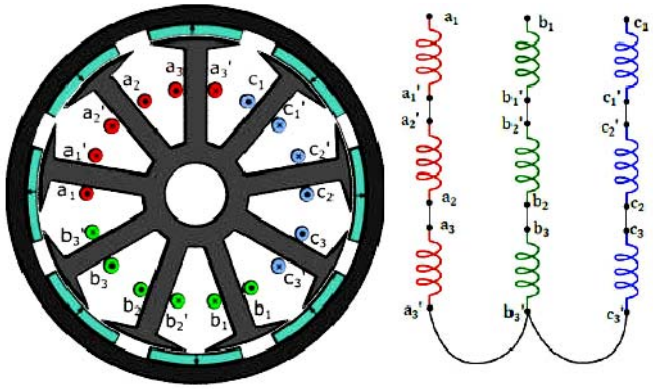

Fig. 2 – Outer surface – PM – rotor brushless actuator (12/10, 12/14).

There are a few main reasons for higher torque density and lower copper (stator) losses:
– Increased number of poles;
– PMs are protected against centrifugal forces;

– Increased airgap diameter (at given overall outer diameter);
– Increased PM flux due to increased airgap area;
– Shorter end-coils due to non-overlapping (tooth wound);
– High overload capacity without PM demagnetization by surface PMs.

These PM electric actuators fulfill the flux-modulation synchronization condition [6, 2].

$$p_a = p_m - p_{PM} > 0 \tag{1}$$

where p_a – main pole pairs of stator winding mmf, p_m – number of stator teeth (with open slots) which play the role of flux modulation (at standstill) with p_m pole pairs; p_{PM} – PM rotor pole pairs.

Highest torque density is obtained with $p_a > 0$ [2].

Sintered NdFeB (B_r=1.2 T) PMs could be used for even more torque density but for small torque (up to a few Nm) and in large fabrication numbers the use of cheap ferrite PMs (B_r=0.45 T) seems practical even in inner IPM rotor actuators Fig. 3 [7].

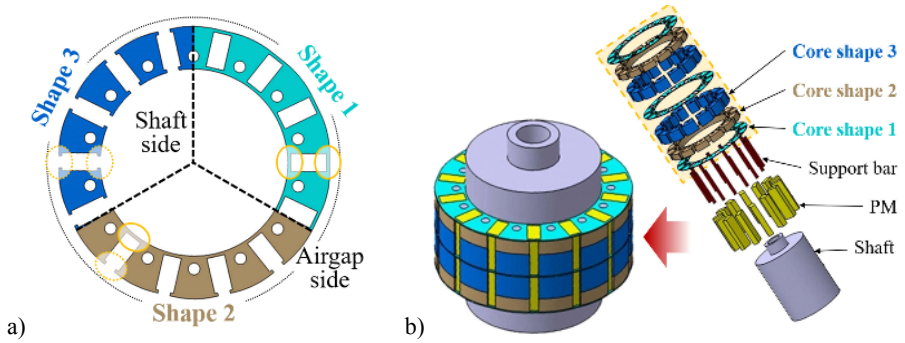

Fig. 3 – Radial – airgap spoke – PM – rotor actuator with rotor multicore, a); structure, b), (after [7]).

The main performance data of such an actuator are summarized in Fig. 4 [7] and Tables 1 and 2 [7].

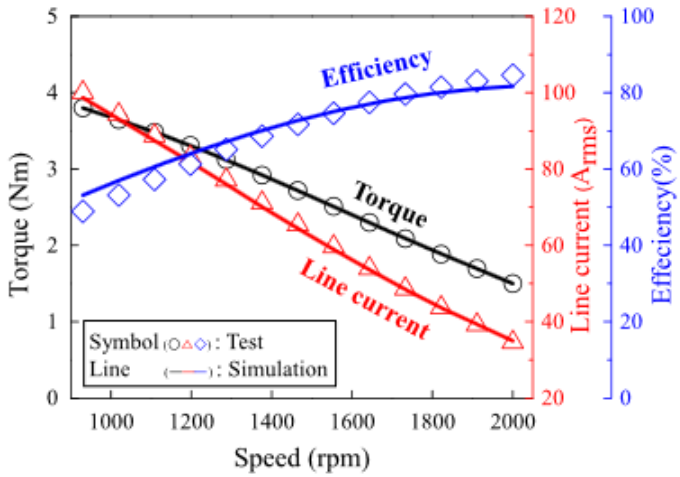

Fig. 4 – Torque, current, efficiency versus speed in 12 Vdc, 1.5 Nm, 2000 rpm radial airgap spoke – PM rotor actuator [7].

Table 1

Comparison of characteristics according to the number of poles and slots

Pole/Slot	Winding factor		LCM	Vibration order
	Fundamental	Sub-harmonic		
12/18	0.866	–	36	6
14/18	0.902	–0.750 (–5/7th)	126	2
16/18	0.945	–0.923 (–5/4th)	144	2

Table 2

Design results of prototype and improved model [7]

QUANTITY	PROTOTYPE	IMPROVED MODEL (MULTI-CORE CFSM)
DC-link voltage (V_{dc})		12
Current limit (Arms)		100
Pole/Slot	16/18	14/18
Stator diameter (mm)		76
Rotor diameter (mm)	50.9	46.6
Stack length (mm)		20.1
Mechanical airgap length (mm)		0.4
Torque density (kNm/m^3)	36.2	41.7 (+15%)

This design [7] illustrated how a notably high torque density at a rather small outer stator core diameter of 76 mm could be obtained by the synergy of multi-core rotor topology with PM flux concentration at a fairly high number of rotor poles at the price of a lower efficiency (82% at 2000 rpm), lower overload capacity and additional cost (by more sintered NdFeB PM weight). It should be noticed that the rated frequency $f_n = 233$ Hz may still be accommodated by 0.3 mm thick regular silicon laminations. With 0.2 mm thick core laminations the efficiency may be further increased by up to 3–4% for the same actuator geometry. The here discussed design resulted also in only 0.6 m/s^2 stator vibration (at $2{\cdot}f_n$ frequency) for 1.5 Nm and 2000 rpm, with an only 0.8% torque ripple, which may be considered very competitive performance.

Further efforts in increasing of torque density with this spoke PM rotor actuator have been reported by adding flux barriers below the spoke PMs to reduce PM flux leakage [8, 9], while a fairly system approach about their design robustness to machine and material properties tolerances is available in [10]. The next competitor in line here is the inner claw-pole stator outer PM rotor actuator.

3.2. Inner claw-pole stator outer PM rather actuators

The recently proposed for multiple applications (robotics included) inner-claw-pole stator-outer-PM-rotor actuator is illustrated in Fig. 5 [11].

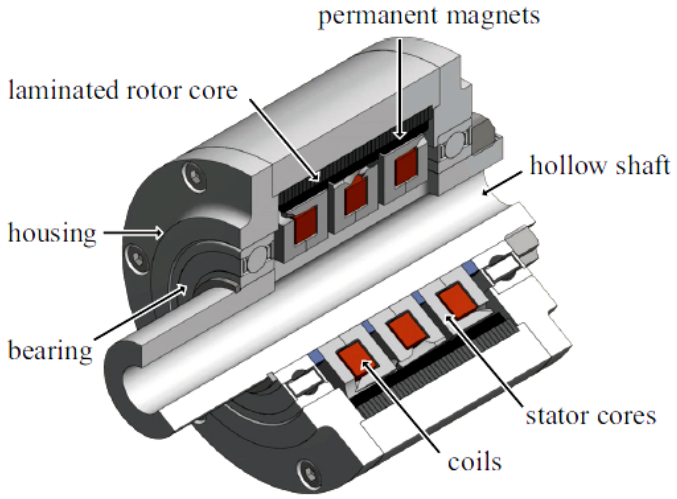

Fig. 5 – Three phase inner-claw-pole stator-outer-PM-rotor actuator [11].

The main merits of such an actuator for robotics (and not only) may be summarized as:

– The inner-claw-pole stator, made of soft magnetic composite (SMC) core (one per phase), with embedded circular-shape a.c. coils (one per phase), results in a modular configuration with $2p$ poles while the outer surface PM pole rotor also produces $2p = 2p_a$ poles, constituting a synchronous machine. The copper weight and losses are minimal (due to coils circularities and their smaller average diameter) for a rather large number of poles $2p \approx 16$–24.

– The pole pitch τ at the airgap should be in general $\tau > 2(g+h_{PM})$; g – the airgap, h_{PM} – radial thickness of PMs, to keep PM fringing acceptably low.
– The fundamental frequency f_n may now go higher than 250 Hz as the mainly hysteresis losses in SMC are lower than core losses in thin laminations at comparable costs.
– The higher airgap diameter allows for high torque density especially when NdFeB sintered magnets are used, while a solid back iron in the rotor may be used also for the outer rotor framing (structure); which may play also the role of a ventilator, provided a suitable dynamic profiling of it is performed.
– The circular shape a.c. coils (one per phase) may be built of copper (or even aluminum) thin sheets (slabs) for higher "slot fill" factor (0.75 instead of 0.5 for round wires) and thus the copper loss (including skin effect) is further reduced.

A typical realization of this actuator has the data in Table 3 and Fig. 6 [11].

Table 3

Outer PM rotor inner claw pole stator actuator dimensions and parameters [11]

Dimensions and parameters	Quantity
Rated speed n_N (rpm)	100
Rated power P_N (W)	120
Rated torque (Nm)	7.53
Current density (A/mm^2)	19.1
Rated frequency (Hz)	16.67
Number of poles	20
Number of turns of winding	167
Rotor outer diameter (mm)	71
Rotor inner diameter (mm)	65
Stator diameter (mm)	60.4
Winding diameter (mm)	40
Main airgap length (mm)	0.3
Stator stack length per phase (mm)	15
Total volume (L)	0.2

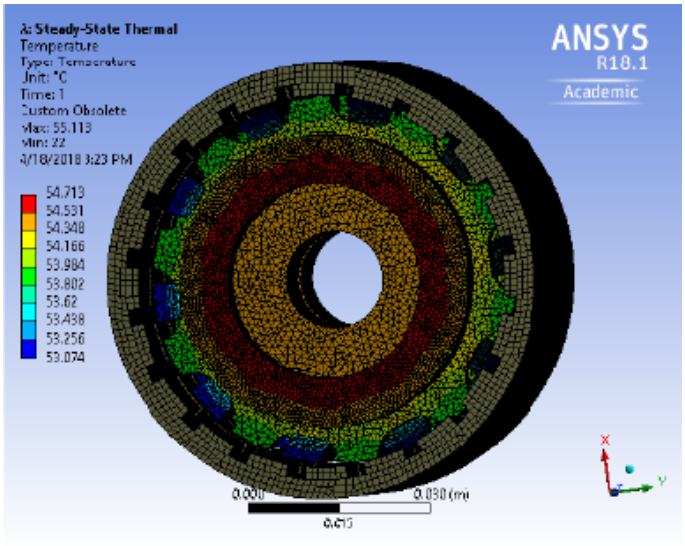

Fig. 6 – Steady state thermal analysis at 19.1 A/mm^2 and 10% duty cycle with no cooling (14 W/m^{2}k) [11].

The electromagnetic and thermal 3D FEM design may be characterized as:

– For j=19.1 A/mm^2 (slot fill factor: 0.7: copper sheets) the stator winding temperature of 123°C (from 20°C) will be reached in 5 minutes while the actuator produces 7.5 Nm average for 129 W of copper loss (at 120°C) for a torque density of 37.65 Nm/l at an outer rotor diameter of 71 mm.

– Reducing the current density to 5 A/mm^2, for a torque of 2.15 Nm, the same actuator, still provides 10.75 Nm/liter of torque for 6.7 W copper loss at 36ºC for full duty cycle and natural air cooling even with 0.5 slot fill factor (copper round wire).
– The SPM rotor allows for high overload without PM demagnetization. Other efforts on outer-PM-rotor inner-claw-pole-stator and other actuators for robotics are described pertinently in [12] (Table 4). They prove notable coherency and thus convey trust in this actuator for robotics.

In addition, for small powers (in the W (subwatt) range) single phase self-starting outer PM rotor inner claw pole stator actuators (Fig. 7) may be preferred [19].

Table 4

Performance of small electric actuator for robotics (edited after [12])

Actuator	Rated torque [Nm]	Airgap diameter [mm]	Stack length (total) mm	Shear stress N/cm^2	Torque density Nm/liter
Transverse flux PM [13]	11	64	90	1.9	n.a
Transverse flux PM [14]	3.4	80	93	3.6	n.a
Claw pole transverse flux PM [15]	2.75	39	60	1.92	n.a
BLDC ILM 70x10 [16]	0.74	50	12.7	1.48	n.a
BLDC EC 90 Flat [17]	0.56	60	13	0.76	n.a
Prototype [12]	0.8	42	35	0.82	9.8
Prototype in [11]	7.5	60 outer rotor diameter 71 outer diameter	3x15	5.89 (for j_{ca}=19.1 A/mm^2 10% duty cycle) 1.69 N/cm^2 for j_{ca}=5A/mm^2 100% duty cycle)	35
Vernier Prototype with q=1 overlapping a.c. coils [18]	26	124	70	n.a	31

Auxiliary slots on stator claw-poles and their skewing leads to lower cogging torque.

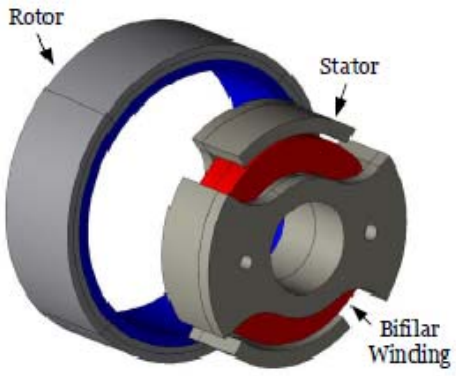

Fig. 7 – Single phase inner-claw pole –stator PMSM [19].

The axial flux PM actuators are now approached.

3.3. Axial flux PM rotor actuators

As the large number of PM poles is allowed for the usual less than 1000–2000 rpm speed (for limited frequency: 500 Hz), the axial flux PM actuator may come into play for robotics. Quite a few topologies have been put forward recently.

Among them we mention here:
– The yokeless-stator (YASA) configurations with twin rotor (Fig. 8a [20]);
– The single-sided axial PM rotor actuator (Fig. 8b) [20];
– The flux-reversal PM rotor actuator (with multiple teeth (slots) on the stator: $2mk$ poles (m – number of phases, k=1, 2, 3) (Fig. 8c) [21].

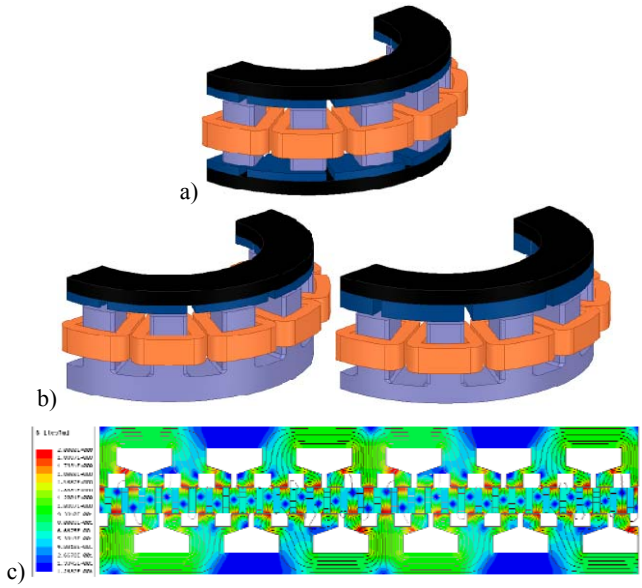

Fig. 8 – Axial flux PM rotor actuators: a) YASA, b) single sided, c) flux-reversal type (with shifted stators).

The three configurations in Fig. 8 are characterized as:
– *YASA*: reduced core loss by lack of stator yoke but more difficult fabrication [22] and good torque density in pancake–like (short length) volume; rolled thin laminated or SMC stator cores are suitable for all axial flux PM actuators.
– *Single sided*: simpler fabrication, good torque density but large axial (uncompensated) force and problems in certifying a certain airgap in contrast to radial airgap actuators.
– *Flux-reversal* type is suitable for even larger number of poles (lower speeds), with a limited number of a.c. coils and larger PM flux concentration via a spoke type PM rotor.
– All the above actuators are found also in the literature as flux – modulation or Vernier machines etc (they all fulfill equation (1) in terms of number of pole pairs of stator mmf (p_a), stator slotting (p_m) and rotor pole pairs (p_{PM})).

The 3D FEM analysis of all these actuators (though forced cooling may suit better, YASA) shows them equivalent in terms of torque density for given geometry (a given number of PM rotor poles). But, as expected, the flux – reversal PM rotor actuators allow for smaller pole pitch (as the stator coils embrace 2(3, 4, 5) elementary (PM) pole pitches) that leads to higher torque density. Thus they may be applied, at lower speeds, to keep the rated fundamental frequency under 500 Hz.

A direct system comparison between various axial flux PM actuators for a given application in terms of torque, speed, efficiency, power factor, active weight and cost, is still due.

Magnetic geared PM actuators follow as the last candidate here, for high torque density, so crucial in robotics applications.

3.4. Magnetic geared PM actuators

A typical, recently proposed, magnetic geared PM actuator (Fig. 9) [23] is characterized by:
– It has 12 stator teeth holding 6 a.c. tooth – wound coils (two per phase, 3 phase);
– It holds on the stator teeth a 27 pole pair stationary PM Halbach array (P_{PMs}=27);
– The outer (variable reluctance, for flux modulation) output rotor holds 31 spaced ferromagnetic (laminated or made of SMC) pieces (p_m=31);

– Inside the outer rotor a 4 pole pair PM Halback array inner high speed rotor is placed (p_{rpm}=4); again $p_{rpm}=p_m-p_{PMs}$.

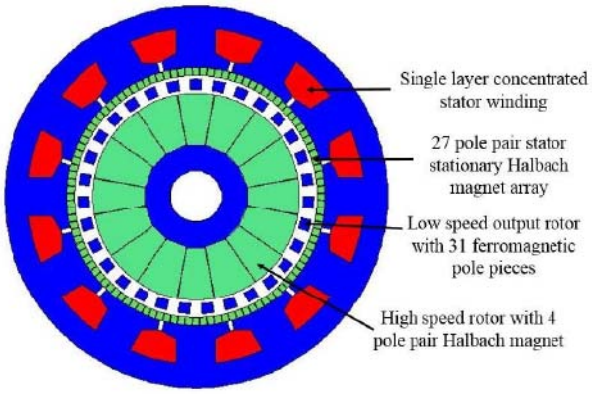

Fig. 9 – A magnetic geared PM actuator (after [23]).

As expected, the number of pole pairs of stator a.c. coils mmf is p_a=4 and interacts synchronously with the inner rotor's p_{rpm}=4 pole pairs; so we deal here with a magnetic gear integrated with a PM synchronous motor.

– Though initially proposed for primary flight control surface (flaps) on aircraft, this configuration, by its low inertia of the load (output) rotor, allows for faster motion control response than perhaps any other configuration shown so far in this paper.
– The magnetic gear effect with a gear ratio of $G=p_m/p_{rpm}=31/4=7.75/1$ is large, which is likely to generate high torque density, at the price of large PM weight (cost) per Nm, though.
– Reference [24] describes in detail recent progress in soft and hard magnetic materials for electric actuators.
– Stator PM electric actuators [2] though deemed here to show lower torque density should not be overlooked.

The case in point [23] refers to an 8.6 Nm, 1200 rpm, only 0.42 kg*cm^2 output (load) rotor inertia magnetic geared PM actuator designed at 62.8 mm outer stator diameter with a 53 mm active (stack) length and 1.05 kg of active weight, developing a large 53.4 Nm/liter torque density for an only less than 8 A/mm^2 rated current density.

The prototype tested, built for an outer diameter of 74 mm for same 53 mm stack length developed at 1200 rpm, 8.00 Nm leading to 43 Nm/liter for measured 160 W of copper losses. So yes, the torque density is high but the copper losses for $8\times2\pi\cdot1200/60=1004.8$ W output power represents already 16% of rated power. As the fundamental frequency $f_{1n}=n_n\times p_n=20\times31=620$ Hz, lower than 1200 rpm speeds of output rotor would benefit from this solution. Also the notable decrease of the torque, developed by the output (low speed) rotor with speed [22], suggests that notable phenomenological aspects still have to be investigated.

The inner high speed rotor (not coupled here to any load) rotates at $n_{HSRn}=n_n\times6=1200$ rpm$\times7.75=9300$ rpm.

It should be noted that there is need for 4 bearings in this rather difficult and costly to fabricate actuator. But the reward in torque density seems staggering.

Note. So far we selected (subjectively though) a few representative PM electric actuators (for less than 100 Nm and less than 2000 rpm) and used results from literature and of our own to characterize them in terms of torque density and copper losses as paramount targets, touching also aspects of thermal behavior and optimal design. With the exception of the Vernier electric actuator in [18], which uses q=1 overlapping a.c. stator coils, all the other configurations in this paper use non-overlapping a.c. coils. But an electric actuator requires PWM converter variable speed control. The selected actuators belonging to 3 phase (or 2×3 phase) electric a.c. machines, if with rather sinusoidal emfs (no load voltages), will require (for low torque ripple) quasi-sinusoidal current control achievable with PWM converters.

While the cost of the PWM converter and its losses depend on the actuator efficiency * power factor, the motion control imposes a plethora of response quality indexes as suggested earlier in the paper.

As quick torque response (in the milliseconds range) is required scalar control strategies ([1, chapter 16]) do not qualify in many robotics applications. But the decoupled flux and torque control methods heritage from electric drives [1] fully qualifies for the job. They are only briefly summarized in what follows by their very recent progress.

4. ADVANCED MOTION CONTROL OF PM ELECTRIC ACTUATORS /RECENT PROGRESS

Notwithstanding that all multi-actuator robots have a centralized (overhead) control system, we will refer here only to the torque, speed and position close-loop (decentralized) control of each 3 (3×2) phase brushless a.c. electric PM actuator.

Remembering the assumed fast millisecond range torque response performance index, we are, in general, restricted to decoupled torque and flux control methodologies, as established through electric drives control heritage [1]:

– Robust field oriented control (FOC) [25];
– Robust direct torque and flux control (DTFC) [26–28];
– Robust feedback linearized control (FLC) [29];
– Best model predictive (and dead bit) control [30].

Also, as most robots in general require, for safety encoders (for position feedback), encoderless control is used at least for redundancy.

Due to space limitations we will insist only on very recent progress in the main encoderless control strategies.

The task is somewhat facilitated by the fact that practically all electric PM actuators in Section 2 are ultimately synchronous machines (even if working on a space harmonic as in flux-modulation configurations) whose emf (no load voltage) is designed close to sinusoidal waveform, with sinusoidal phase currents, to reduce torque ripple and additional core and PM losses. Two 3 phase windings are proposed only for safety critical applications, as a simplified fault tolerance option. Multiphase (5, 7, 9 phases) a.c. PM actuators [1, Chapter 16] are not treated here though they allow, by reconfigurable control, more fault tolerance at the price of notably increased complexity (cost). As advanced FOC of brushless a.c. electric PM actuators and DTFC are rather equivalent (in performance) while the latter is more robust and simpler, in encoderless implementation with larger inductance (in p.u.) PM brushless actuators , we will deal directly only with DTFC here.

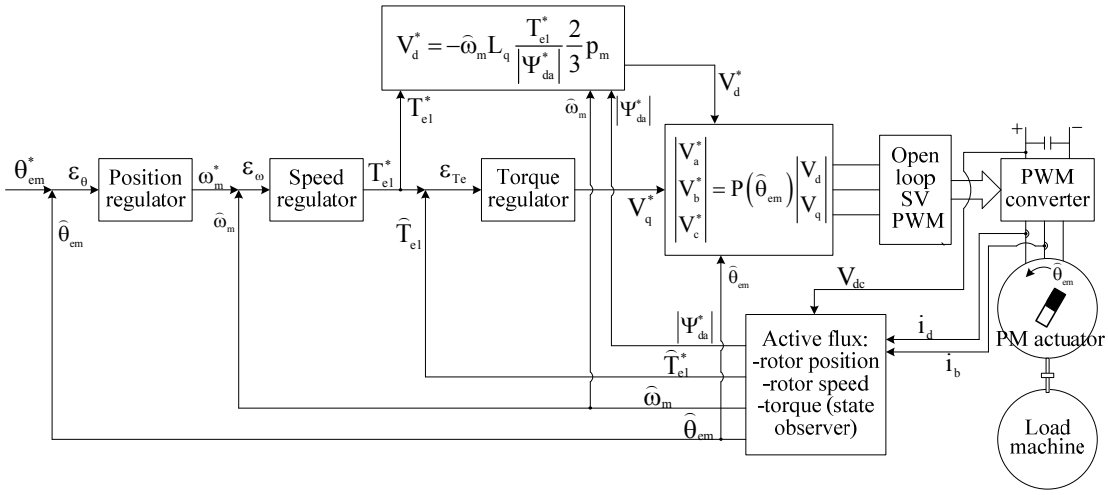

Fig. 10 – Generic (potential) "active flux" encoderless DTFC of electric PM actuators, with id=0.

4.1. Robust DTFC of brushless 3 phase a.c. electric PM actuators

As 3 phase equivalent synchronous machines, the electric PM actuators operate at the speed $n_m=f_a/p_m$ (f_a – fundamental frequency of stator phase voltages, p_m – number of pole pieces of flux-modulator (output) rotor).

With sinusoidal emf E_1 and considering only the stator winding working (maximum winding factor) space harmonic, the electric PM actuator may be described by the space vector (orthogonal) model, typical to PM synchronous motors [1]) in output rotor coordinates (ω_{em}):

$$\begin{aligned}
&\bar{i}_s R_s - \bar{V}_s = -\frac{\partial \bar{\Psi}_s}{\partial t} - j\omega_{em}\bar{\Psi}_s; \quad \bar{V}_s = V_d + jV_q; \quad \bar{i}_s = i_d + ji_q;\\
&\bar{\Psi}_s = \Psi_d + j\Psi_q; \quad T_{e1} = \frac{3}{2}p_m\left(\Psi_d i_q - \Psi_q i_d\right); \quad \Psi_d = \Psi_{\mathrm{PMd}} + L_d i_d;\\
&\Psi_q = L_q i_q; \quad \frac{J}{p}\cdot\frac{\mathrm{d}\omega_{em}}{dt} = T_{e1} - T_{\mathrm{load}} - T_{\mathrm{cogg}}(\theta_{em}) - B\omega_m;
\end{aligned} \tag{2}$$

where T_{cogg} – cogging torque, T_{load} – load torque

$$\frac{\mathrm{d}\omega_{em}}{\mathrm{d}t} = \theta_{em}; \quad \omega_{em} = 2\pi n_n \cdot p_m \tag{3}$$

$$\bar{V}_s = \frac{2}{3}\left(V_a(t) + V_b(t)e^{j\frac{2\pi}{3}} + V_c(t)e^{-j\frac{2\pi}{3}}\right)e^{j\theta_{em}} \tag{4}$$

with ω_{em} – electrical synchronous angular speed; V_a, V_b, V_c – the instantaneous phase voltages (phase terminal to null point); the Park transform (4), in output rotor coordinates, is also valid for stator phase currents i_a, i_b, i_c and phase flux linkages Ψ_a, Ψ_b, Ψ_c.

Core losses, PM losses and additional torque pulsations (except for zero stator current (cogging) torque T_{cogg} (ω_{em})) are not included in the above model, which is, however, sufficient for dynamics and control system design.

In general d and q axis inductances L_d and L_q are different from each other and dependent on i_d, i_q current components (the so called cross-coupling saturation effect).

To simplify both the encoder and encoderless FOC we recall here the "active flux" concept [31], $\bar{\Psi}_{da}$, always in axis d (irrespective of load) – in absence of crosscoupling saturation, when the rotor position estimation error has to be corrected:

$$\bar{\Psi}_{da} = \Psi_S - L_q i_s; \quad \bar{\Psi}_{da} = \Psi_{da} + j\cdot 0\,. \tag{5}$$

Now the torque expression (2) reduces to:

$$T_{\mathrm{e1}} = \frac{3}{2}p_m\Psi_{da}i_q; \quad \Psi_{da} = \Psi_{\mathrm{PMd}} + \left(L_d - L_q\right)i_d\,. \tag{6}$$

And the voltage equation (2) reduces to:

$$\bar{i}_s\left(R_s + (s + j\omega_m)L_q\right) - \bar{V}_S = -\bar{\Psi}_{da}\left(s + j\omega_m\right). \tag{7}$$

Equation (7) shows that the "active flux" model/concept *"turns" the salient pole rotor* model into a *functionally non-salient pole rotor* model with L_q as its inductance.

The active flux vector angle corresponds to rotor position even at zero speed (if a small saliency of at least: $L_d/L_q < 0.9$ is available) when signal injection voltages are supplied to the stator windings.

Most robotics electric PM actuators in section II have such a small physical saliency which also leads to one more simplification: they may be controlled at (close to) $i_d \approx 0$ if no flux weakening (extended) speed range at constant power is needed. Also, for $i_d = 0$, $\Psi_{da} = \Psi_{\mathrm{PMd}}$.

In such a condition ($i_d = 0$) let us introduce in Fig. 10 an "active – flux" based generic DTFC control structural diagram for a PM electric actuator (Fig. 10).

The key component of the control is the active flux state observer which estimates the latter on-line (during (20–30)% of inverter switching time T_{sw}) and contains:

– The active flux $\bar{\Psi}_{da}$ estimation;

– Rotor electrical position $\hat{\theta}_{em}$ estimation;

– The rotor electrical speed $\hat{\omega}_m$ estimation;

– The torque $\hat{T}_{e1}$ estimation.

A typical such robust state observer is shown in Fig. 11.

The entire control system is characterized by: A cascaded position, speed and direct torque control strategy where at least the torque regulator is based on the "supertwisting sliding mode (ST-SM)" [32] principle, where the command output V_q^* is:

$$V_q^* = -A\sqrt{|\varepsilon_{Te}|}\,\text{sigmoid}(\varepsilon_{Te}) + V_0;\quad \frac{dV_0}{dt} = -B * \text{sigmoid}(\varepsilon_{Te}). \tag{8}$$

ST-SM provides for a second order sliding mode (SM) behavior without chattering, while also avoiding the calculation of the time derivative of torque error $\varepsilon_{Te} = T_e^* - T_e$.

The typical voltage and current "active flux" model observer in Fig. 11 contains a PLL motion based additional part, to secure smaller position and speed errors during motion transients and load torque perturbations. Besides, the PLL observer in Fig. 11 yields the estimated speed ω_{em} too.

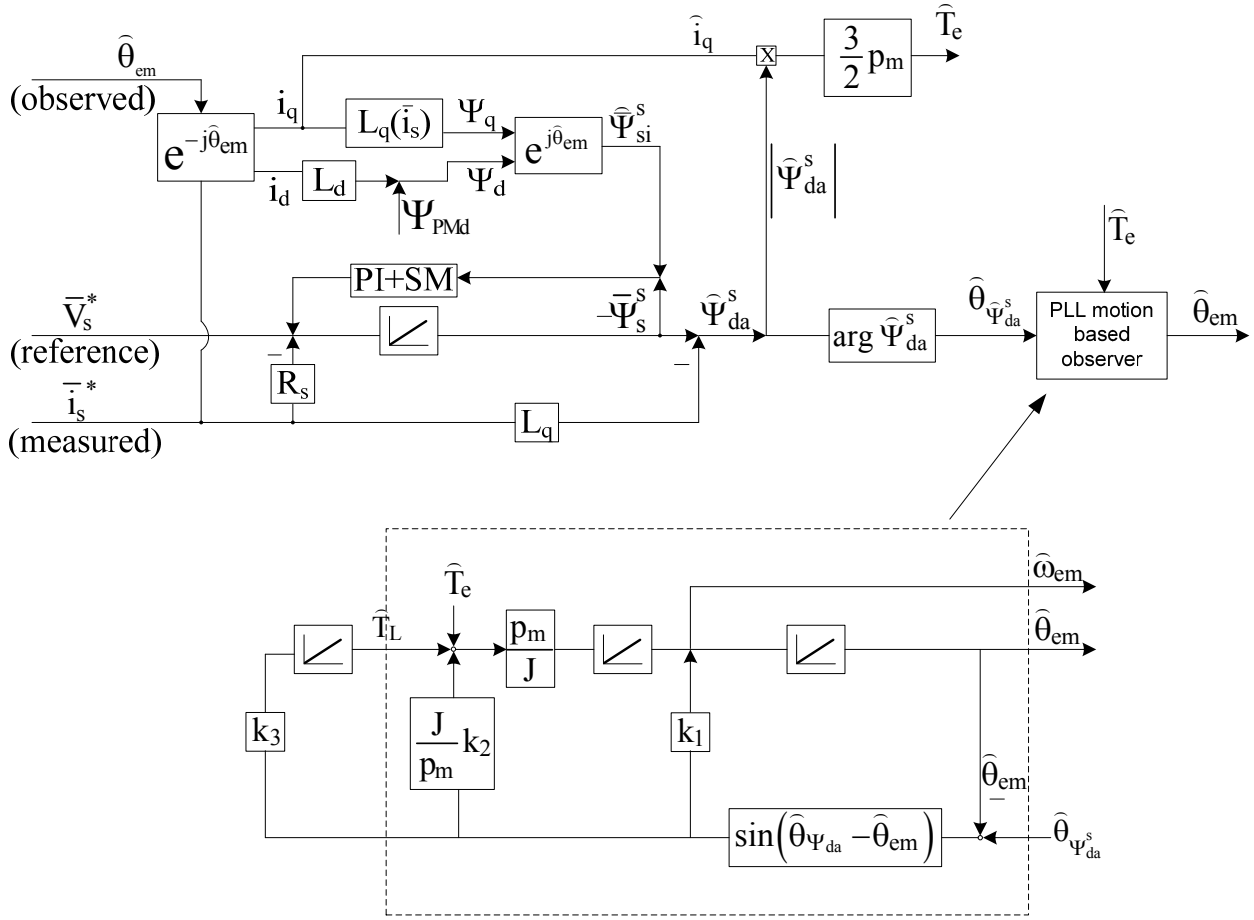

Fig. 11 – Active flux based state observer for electric PM actuator.

The PI + SM (sliding mode) compensator between the voltage and current model (Fig. 11) provides for better behavior at small speeds and during actuator parameters variations when the latter are not compensated for.

The estimated active flux amplitude $\left|\hat{\Psi}_{da}\right|$ is used to feedforward V_d^* (for i_d=0) while also may "take care" of PM flux linkage variations due to temperature ($\Psi_d^a = \Psi_{\text{PMd}}$, for i_d=0).

The scheme may work even for surface – PM rotor electric actuators, except for very low speeds.

Typical experimental results, with a similar encoderless control scheme as in Figs. 10–11, [33], are shown in Fig. 12 for torque response and for wide speed range response (at constant stator flux Ψ_s, though).

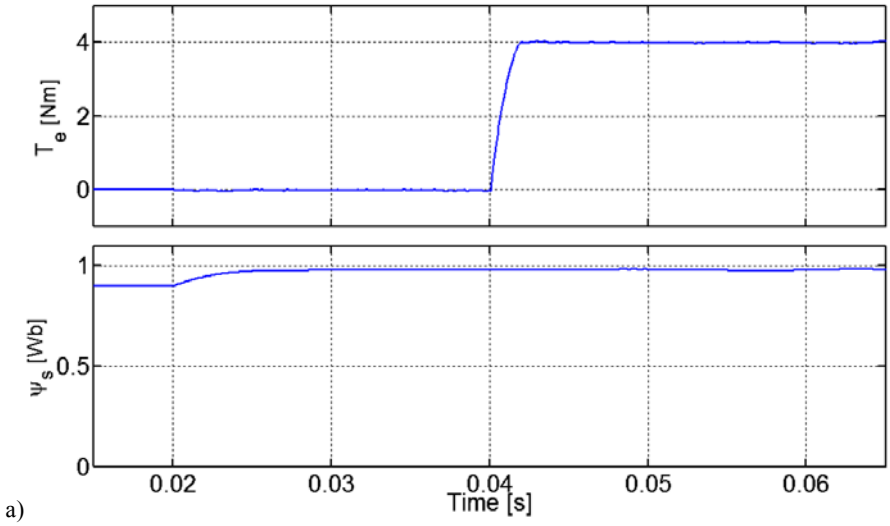

a)

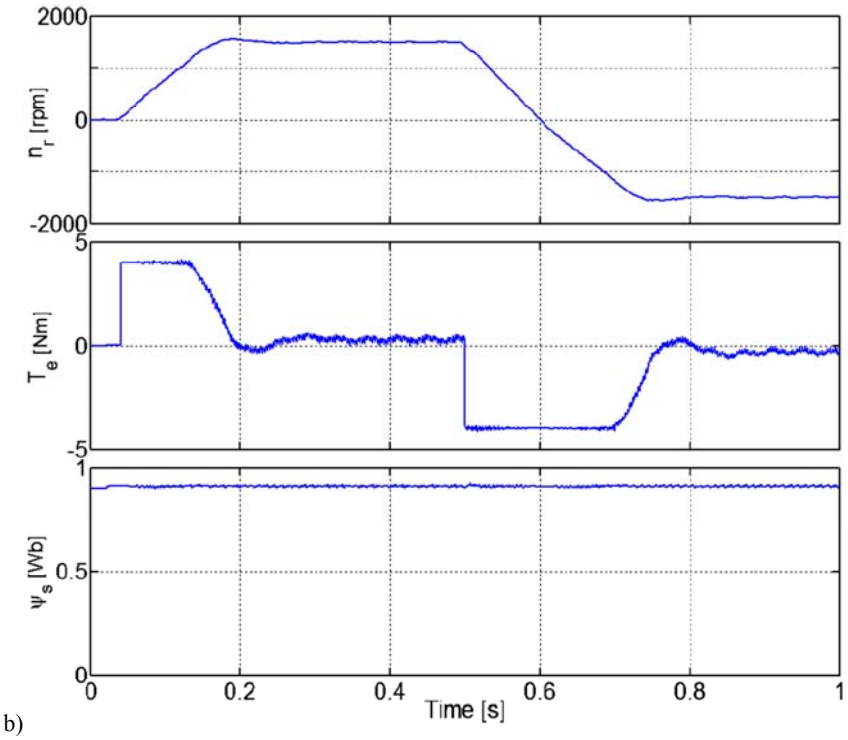

b)

Fig. 12 – Super-twisting sliding mode control of encoderless torque and flux in a PM brushless actuator, based on "active flux" concept (after [33]): a) fast torque transients response; b) speed transients response.

Similar experimental results for DTFC active flux based encoderless control of a PM electric actuator operating at 2 rpm are shown in Fig. 13 [34]. No signal injection is yet used. When used, even operation at zero speed with full step torque perturbation is feasible [35].

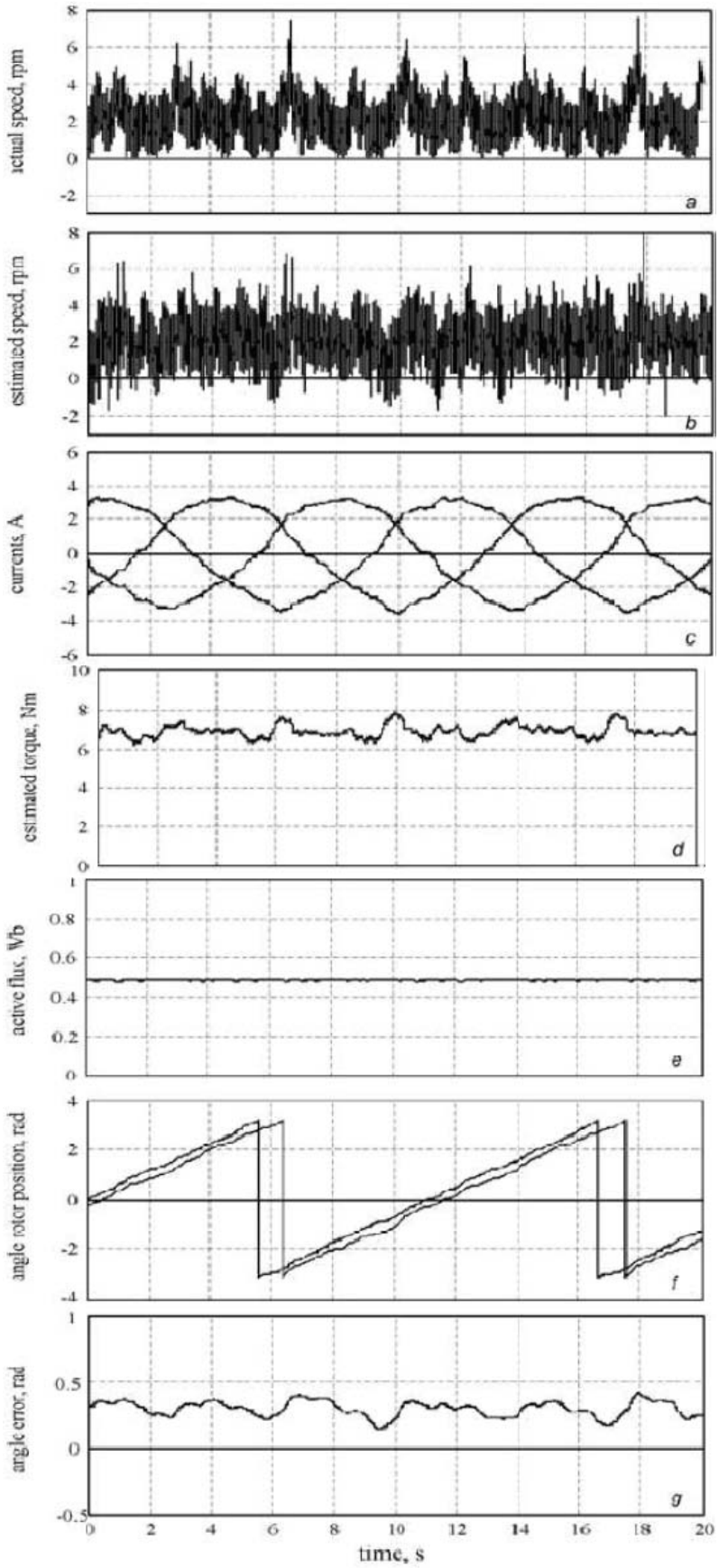

Fig. 13 – Encoderless active flux based DTFC of PM electric actuator operation at 2 rpm – experimental, without signal injection [34].

4.2. Feedback linearization control (FLC)

With Ψ_s^2 and T_e as variables (FLC) has been proposed to simplify the control system design of DTFC of PM electric actuators. Robustness has been provided by using two sliding mode observers for nonlinear parts [36]:

$$F_s = \Psi_s^2 = \Psi_d^2 + \Psi_q^2$$

$$\frac{\mathrm{d}T_e}{\mathrm{d}t} = \overbrace{-\frac{R_s}{L_s}T_e}^{\text{linear part}} + \overbrace{k_T\left(V_q - \omega_m \Psi_d\right)}^{W_q\,(\text{nonlinear part})};\quad k_T = \frac{3}{2}p_m\frac{\Psi_{PM}}{2L_s} \tag{9}$$

$$\frac{\mathrm{d}F_s}{\mathrm{d}t} = \overbrace{-\frac{2R_s}{L_s}F_s}^{\text{linear part}} + \overbrace{\frac{2R_s}{L_s}\Psi_{PM}\Psi_d + 2\Psi_d V_d + 2\Psi_s V_q}^{W_d\,(\text{nonlinear part})}.$$

The nonlinear parts $\hat{W}_d$, $\hat{W}_q$ are estimated using sliding mode (SM):

$$\begin{aligned}\hat{W}_d &= k_{Vq}\,\mathrm{sign}\left(F_s^* - F_s\right) + PI\left(F_s^* - F_s\right)\\ \hat{W}_q &= k_{Vd}\,\mathrm{sign}\left(T_e^* - \hat{T}_e\right) + PI\left(T_e^* - \hat{T}_e\right)\end{aligned}. \tag{10}$$

The reference voltages V_d^*, V_q^* are then calculated with estimated $\hat{W}_d$, $\hat{W}_q$ defined in (9).

Via Lyapunov criterion the stability is secured if [36]:

$$K_{Vq} > \frac{1}{T_S}T_{e\max};\quad K_{Vd} > \frac{2}{T_S}F_{s\max}. \tag{11}$$

Typical results for torque and speed responses are visible in Fig. 14 a,b, again for encoderless control at rather low speeds [36].

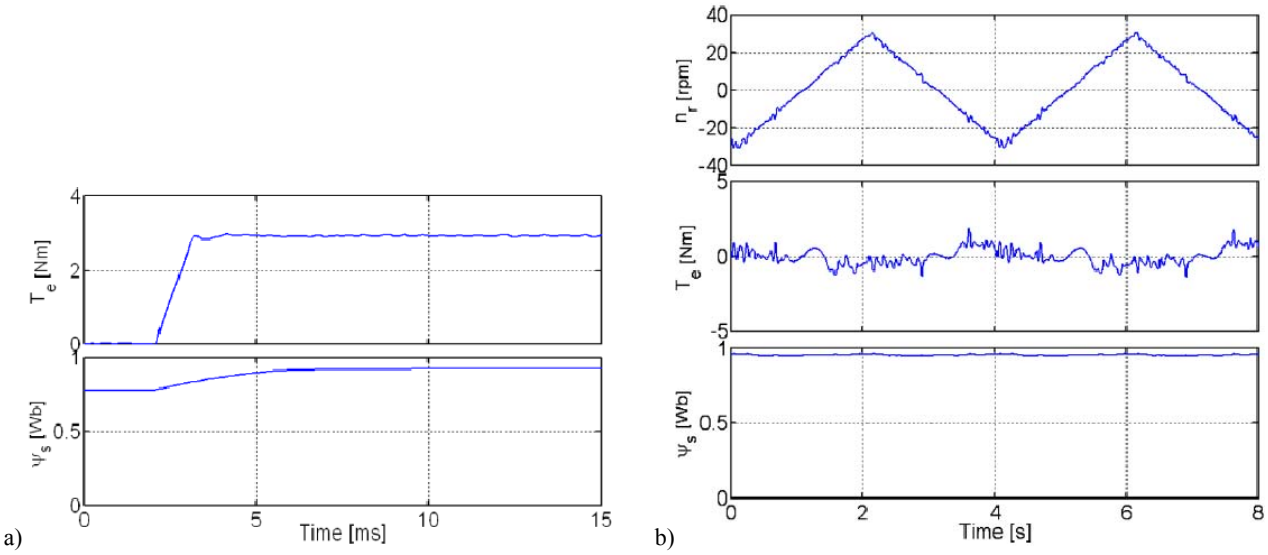

Fig. 14 – Encoderless feedback linearization DTFC of an electric PM actuator with PI+SM observers for the nonlinear parts $\hat{W}_d$, $\hat{W}_q$: a) torque transient response; b) low speed transients [36].

Fast millisecond range in torque bandwidth is visible even at very low speeds. As expected, the behavior will be even better with encoder feedback.

4.3. Robust model predictive FOC of electric PM actuators

Model predictive control is used associated with FOC or DTFC in an effort to simplify the control system, by choosing the over a small sampling time optimal voltage vector in the PWM converter (out of 6 nonzero and 2 zero such vectors, typical to a 2 level voltage source converter; more voltage vectors are available in 3, 5 voltage level PWM converters).

The optimal voltage vector candidate is obtained based on an optimization (energy) criterion F_0 such as:

$$F_{0\min} = \min\left(\left| \frac{T_e^* - \hat{T}_e}{T_e^*} \right|^2 + (1 - c_1) \left| \frac{\Psi_s^* - \hat{\Psi}_s}{\Psi_s^*} \right|^2 \right) \tag{12}$$

for torque mode control.

Then the discretised actuator equations are solved for 1, 2, 3 time horizons (samples) and for all available voltage vectors. The chosen voltage vector is the one which makes F_0 minimum.

Yes, stability has to be checked, but, also, since the MPC is model based, for robustness it requires online corrections of PM actuator electrical and mechanical parameters.

For example, simplified repetitive MPC of an electrical PM actuator is proposed in [37] to adjust (compensate) for parameters mismatch and current distortion.

From voltage equation in (2) the discrete dq current prediction is:

$$\begin{aligned} \hat{i}_{dq}(k+1) &= \hat{i}_{dq}(k) + L_s^{-1} T_s \left[V_{dq}(k) - R_s i_{dq}(k) - j\omega_{em} \hat{\Psi}_{dq}(k) \right] \\ \hat{\Psi}_{dq}(k) &= L_s \hat{i}_{dq}(k) + \Psi_{PM} \end{aligned} \tag{13}$$

A second prediction is required due to one step delay in $\Psi_{dk}(k)$; with $\hat{i}_{dq}(k+2) \approx i_{dq}^*(k+1)$ we get the predictive current

$$\hat{i}_{dq}(k+2) = \hat{i}_{dq}(k+1) + L_s^{-1} T_s \left[V_{dq}^*(k+1) - R_s \hat{i}_{dq}(k+1) - j\omega_{em} \Psi_{dq}(k+1) \right]. \tag{14}$$

From (13) the reference voltage $V_{dq}^*(k+1)$ is:

$$V_{dq}^*(k+1) = R_s \hat{i}_{dq}(k+1) + L_s T_s^{-1} \left[i_{dq}^*(k+1) - \hat{i}_{dq}(k+1) \right] + j\omega_{em} \Psi_{dq}(k+1) \tag{15}$$

with $i_{dq}^*(k+1) \approx (1 + k_i) i_{dq}^*(k) - k_i i_{dq}^*(k-1); \quad 0 < k_i < 1$.

Also, due to dead beat strategy: $i_{dq}^*(k+1) \approx \hat{i}_{dq}(k+1)$.

Now the voltage vector that produces minimum F_0 (12) is chosen, starting from the above mentioned MPC model.

The simplified (compensated against quantized error) repetitive resonant feedforward control against disturbances is presented in detail in [37].

Sample experimental results [37] with simplified feedforward dual (first and second resonant MPC) repetitive control on top of FOC – Fig. 15 – refer to i_d and i_q current pulsation reduction for mismatched stator resistance ($4R_s$) synchronous inductance ($0.85L_s$) and PM flux linkage ($0.85\Psi_{PM}$) and illustrate the beneficial effect of simplified repetitive control (SRC2) on i_d and i_q (cleaning) and thus an actuator performance (from 2.8% to 1.75% stator current THD) and lower copper losses.

Still more progress in robust control is needed as even for the combined voltages plus current model state observer is hard to alleviate closed loop speed oscillations due to dc offsets [37], besides the urge to increase immunity to electric actuator parameters etc. [38–41].

Final note on control:

As expected the discussion on control should continue on issues such as, but not limited to:

– digital implementation software and hardware;

– fault tolerance aspects;

– control precision and dynamic robustness;
– reliability of electric – PM actuator systems etc.
However, due to lack of space we stop here on the subject.

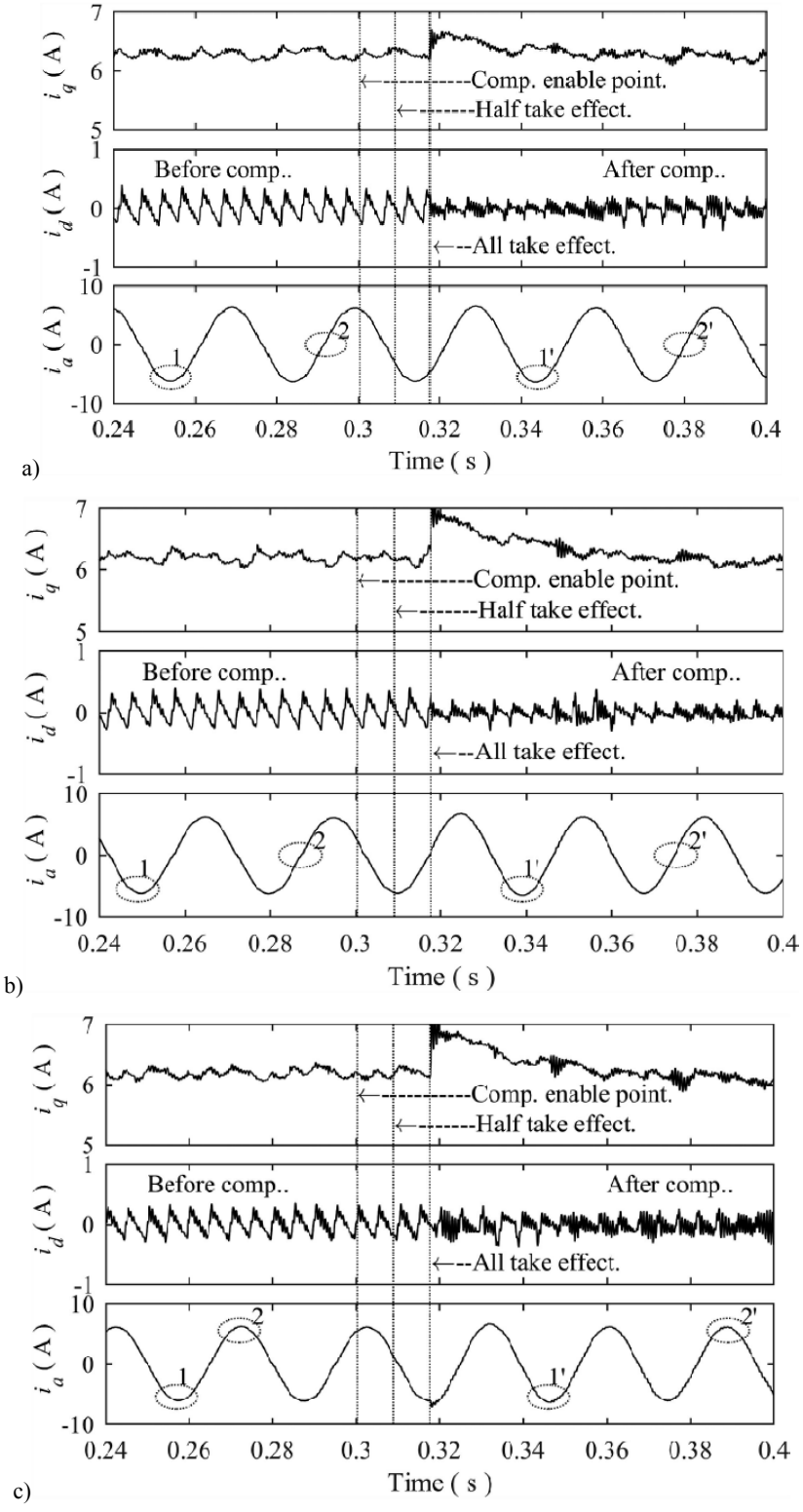

Fig. 15 – Experimental i_d, i_q, i_a (phase a current) for simplified repetitive MDC of an electric PM actuator at 500 rpm: a) for $R_s \rightarrow 4R_s$; b) $L_s \rightarrow 0.85\,L_s$; c) $\Psi_{PM} \rightarrow 0.85\Psi_{PM}$ [37].

5. CONCLUSION

The present review paper leads to final remarks such:

– Multiple performance criteria – energy conversion, response performance and weights and costs – are needed to assess robotics actuator drives.
– Considering high torque density and low loss/torque as paramount in robotics drive only four PM electric actuators topologies have been singled out and analyzed with sample performance illustrations.
– Assuming that fast/non-hesitant robust torque response is key metric for robotics drives only DTFC with advanced encoderless (even only for redundancy) of brushless PM electric actuators has been treated in detail with sample results including feedback linearization and model based predictive implementation of their control.
– Recent progress in power converters for electric PM actuators should/will be treated in a separate thorough investigation.

REFERENCES

1. I. BOLDEA, S.A. NASAR, *Electric Drives*, 3rd edition, CRC Press, Florida, USA, 2017.
2. I. BOLDEA, L. TUTELEA, *Reluctance electric machines design and control*, CRC Press, Florida, USA, 2019.
3. H. MOAYED-JAHROMI, A. RAHIDEH, M. MARDANEH, *2-D analytical model for external rotor brushless PM machines*, IEEE Trans. on Energy Conversion, **EC-31**, *3*, pp. 1100-1109, 2016.
4. I. PETROV, M. NIEMELA, P. PONOMAREV, J. PYRHONEN, *Rotor surface ferrite PMs in electric machines: advantages and limitations*, IEEE Trans. on Industrial Electronics, **IE-64**, *7*, pp. 5314-5322, 2017.
5. A. ISFANUTI, L.N. TUTELEA, I. BOLDEA, T. STAUDT, P.E. DA SILVA, *Outer ferrite-PM-rotor BLAC motor characterization: FEM assisted optimal design*, Record of 2018 XIII International Conference on Electrical Machines (ICEM), Alexandroupoli, Greece, 2018.
6. D. LI, R. QU, J. LI, *Topologies and analysis of flux modulation machines*, Record of 2015 IEEE Energy Conversion Congress and Exposition (ECCE), pp. 2153-2160, 2015.
7. M.-R. PARK, J.-W. JUNG, D.-Y. KIM, J.-P. HONG, M.-S. LIM, *Design of high torque density multicore concentrated flux-type synchronous motor considering vibration characteristics*, IEEE Trans. on Industry Applications, **IA-55**, *2*, pp. 1351-1359, 2019.
8. E. CARRARO, N. BIANCHI, S. ZHANG, M. KOCH, *Design and performance comparison of fractional slot concentrated winding space – type synchronous motors with different slot-pole combinations*, IEEE Trans. on Industry Applications, **IA-54**, *3*, pp. 2276-2284, 2018.
9. W. LIU, T.A. LIPO, *Analysis of consequent pole spoke type Vernier permanent magnet machine with alternating flux barrier design*, IEEE Trans. on Industry Applications, **IA-54**, *6*, pp. 5918-5929, 2018.
10. N. TARAN, V. RALLABANDI, D.M. IONEL, P. ZHOU, M. THEILE, G. HEINS, *A systematic study on the effects of dimensions and materials tolerances on PMSMs based on the IEEE Std 1812*, IEEE Trans. on Industry Applications, **IA-55**, *2*, pp. 1360-1371, 2019.
11. J. LIANG, A. PARSAPOUR, E. COSOROABA, M. WU, I. BOLDEA, B. FAHIMI, *A high torque density outer rotor claw pole stator PMSM*, Record of 2018 IEEE Transportation Electrification Conference and Expo (ITEC), pp. 389-393, 2018.
12. M. KELLER, S. MULLER, N. PARSPOUR, *Design of a PM excited transverse flux machine for robotics applications*, Record of 2016 XXII International Conference on Electrical Machines (ICEM), pp. 1522-1527, 2016.
13. F. DREHER, N. PARSPOUR, *A novel high speed PM claw pole transverse flux machine for use in automotion*, Record of IEEE – SPEEDAM, pp. 1240-1245, 2012.
14. Y. GUO, J.G. ZHU, P.A. WATTERSON, W. WU, *Development of a PM transverse flux motor with SMC core*, IEEE Trans. on Energy Conversion, **EC-21**, *2*, pp. 426-434, 2006.
15. Y. SHEN, Z.Q. ZHU, J.T. CHEN, R.P. DEODHAR, A. PRIDE, *Analytical modeling of claw pole stator SPM brushless machine having SMC stator core*, IEEE Trans. on Magnetics, **MAG-49**, *7*, pp. 3830-3833, 2013.
16. Robodrive TQ-Systems GmBH, [online]: http://www.robodrive.com/en/products/stamp/stamp.jsp, 2016, accessed January 2020.
17. Maxon Motor AG, [online]: https://www.maxongroup.com/maxon/view/content/ec-flat-motors, 2016, accessed January 2020.
18. K. XIE, D. LI, R. QU, X. REN, Y. PAN, *A new perspective on SM Vernier machine mechanism*, IEEE Trans. on Industry Applications, **IA-55**, *2*, pp. 1420-1429, 2019.
19. S. LEITNER, H. GRUEBLER, A. MUETZE, *Cogging torque minimization on a mass-produced sub-fractional horsepower brushless direct current claw pole motor*, Record of IEEE Energy Conversion Congress and Exposition (ECCE), pp. 6083-6089, 2018.
20. M. TARAN, G. HEINS, V. RALLABANDI, D. PATTERSON, D.M. IONEL, *Torque production capability of axial flux machines with single and double rotor configurations*, Record of IEEE Energy Conversion Congress and Exposition (ECCE), pp. 7336-7341, 2018.
21. V. RALLABANDI, M. TARAN, D.M. IONEL, I. BOLDEA, *Axial-flux PM synchronous machines with airgap profiling and very high ratio of spoke rotor poles to stator concentrated coils*, Record of 2017 IEEE International Electric Machines and Drives Conference (IEMDC), 2017.

22. H. VANSOMPEL, A. YARANTSEVA, G. CROEVECOEUR, *An inverse thermal modeling approach for thermal parameter and loss identification in an axial flux PM machine*, IEEE Trans. on Industrial Electronics, **IE-66**, *3*, pp. 1727-1735, 2019.
23. R. DRAGAN, R.E. CLARK, E.K. HUSSAIN, K. ATALLAH, M. ODAVIC, *Magnetically geared pseudo direct drive for safety critical applications*, IEEE Trans. on Industry Applications, **IA-55**, *2*, pp. 1239-1249, 2019.
24. N. LEUNING, S. ELFGEN, B. GROSCHUP, G. BAVENDIEK, S. STEENTJES, K. HAMEYER, *Advanced soft and hard magnetic material models for the numerical simulations of electrical machines*, IEEE Trans. on Magnetics, **MAG-54**, *11*, p. 8107008, 2018.
25. F. BLASCHKE, *The principle of field orientation as applied to the new transvector closed-loop system for rotating-field machines*, Siemens Review, **34**, *3*, pp. 217-220, 1972.
26. I. TAKAHASHI, T. NOGUCHI, *A new quick-response and high efficiency control strategy of an induction motor*, IEEE Trans. on Industry applications, **IA-22**, *5*, pp. 820-827, 1986.
27. M. DEPENBROCK, *Direct self-control (DSC) of inverter fed induction machine*, IEEE Trans. on Power Electronics, **PE-3**, *4*, pp. 420-429, 1988.
28. I. BOLDEA, S.A. NASAR, *Torque vector control (TVC) – a class of fast and robust torque, speed and position digital controllers for electric drives*, EMPS Journal, **15**, *3*, pp. 135-147, 1988.
29. D.L. SOBCZUK, *Nonlinear control of PWM inverter fed IM drives*, Record of IEEE – ISIE, Vol. 2, pp. 958-962, 1996.
30. J. RODRIGUEZ, P. CORTEZ, *Predictive control of power electronics and electric drives*, IEEE, Wiley, 2012.
31. I. BOLDEA, M.C. PAICU, G.D. ANDREESCU, *Active flux concept for motion sensorless unified AC drives*, IEEE Trans. on Power Electronics, **PE-23**, *5*, pp. 2612-2618, 2008.
32. A. LEVANT, *Sliding order and sliding accuracy in sliding mode control*, Int. Journal of Control, **58**, *6*, pp. 1247-1263, 1993.
33. C. LASCU, I. BOLDEA, F. BLAABJERG, *Super-twisting sliding mode control of torque and flux in PMSM drives*, Record of IECON 2013-39th Annual Conference of the IEEE Industrial Electronics Society, pp. 3171-3176, 2013.
34. I. BOLDEA, S. AGARLITA, L. TUTELEA, *The active flux concept for motion sensorless unified AC drive: a tutorial review*, Record of IEEE – ACEPM – OPTIM, 2011.
35. S. AGARLITA, I. BOLDEA, F. BLAABJERG, *High frequency injection assisted "active flux"-based sensorless vector control of reluctance synchronous motors, with experiments from zero speed*, IEEE Trans. on Industry Applications, **IA-48**, *6*, pp. 1931-1939, 2012.
36. C. LASCU, I. BOLDEA, F. BLAABJERG, *Direct torque control via feedback linearization for PMSM drives*, Record of 2012 13th International Conference on Optimization of Electrical and Electronic Equipment (IEEE – OPTIM), pp. 338-343, 2012.
37. Y. LIU, SH. CHENG, B. NING, Y. LI, *Robust model predictive control with simplified repetitive control for electric machine drives*, IEEE Trans. on Power Electronics, **PE-34**, *5*, pp. 4524-4535, 2018.
38. G.J. JO, J.W. CHOI, *Gopinath model-based voltage model flux observer design for FOC of IM*, IEEE Trans. on Power Electronics, **PE-34**, *5*, pp. 4581-4592, 2019.
39. D. WANG, K. LU, P.O. RASMUSSEN, *Improved closed loop flux observer based sensorless control against system oscillations for synchronous reluctance machine drives*, IEEE Trans. on Power Electronics, **PE-34**, *5*, pp. 4593-4602, 2019.
40. R. YANG, M. WANG, L. LI, Y. ZENGGU, J. JIANG, *Integrated uncertainty disturbance compensation with second-order sliding-mode observer for PMLSM-driven motion stage*, IEEE Trans. on Power Electronics, **PE-34**, *3*, pp. 2597-2607, 2019.
41. R.D. LORENZ, *Robotics and automation applications of drives and converters*, Proceedings of the IEEE, **89**, *6*, pp. 951-962, 2001.

Received January 23, 2020